Variable-area resonant tunneling diodes using implanted in-plane gates

C. J. Goodings
Microelectronics Research Centre, Cavendish Laboratory, Madingley Road, Cambridge CB3 0HE, United Kingdom

H. Mizuta
Advanced Devices Research Department, Central Research Laboratory, Hitachi Ltd., Kokubunji 185, Tokyo, Japan

J. R. A. Cleaver and H. Ahmed
Microelectronics Research Centre, Cavendish Laboratory, Madingley Road, Cambridge CB3 0HE, United Kingdom

(Received 30 August 1993; accepted for publication 4 April 1994)

Variable-area resonant tunneling diodes have been fabricated using a process in which the lateral confinement is produced by an in-plane implanted gate. The basic operation of such devices is discussed, and the lateral confinement shown by both measurements and numerical modeling to be very nearly symmetrical about the resonant tunneling diode (RTD) barriers. Fine structure has been observed near threshold for relatively large area devices and this has been attributed to single-electron or few-electron tunneling through donor states in the quantum well. Additional fine structure seen in the valley current of small-area devices has been shown to be consistent with the effects of lateral quantization in the system. Finally, results are presented for strip devices in which the resonant tunneling peak breaks up into numerous subpeaks on application of the gate voltage, and this is attributed to pinning of the confining potential by donors close to the RTD barriers.

I. INTRODUCTION

The topic of small-area resonant tunneling diodes (RTDs) has become of great interest recently, especially for the study of electron systems with reduced dimensionality. The majority of such systems are fabricated by the production of fine pillar structures in which the lateral confinement is produced by the depletion resulting from surface states.[1–5] Lateral confinement produced by ion damage has also been reported.[6] Such methods have the common feature that the degree of confinement is fixed: in one dimension by the growth of the double barriers in the RTD material and in the other two dimensions by the physical structure of the device. Thus, the most important parameters for any quantum effects, the location and the magnitude of the confinement potential, cannot be varied. Devices based on resonant tunneling material in which the lateral confinement can be controlled electrically have advantages over their fixed-area counterparts for the study of electron systems with reduced dimensions.

Recently, pioneering work has been reported on three-terminal RTD devices in which the electrical confinement is produced by placing a surface gate just above the RTD double barriers to deplete the underlying material. Such structures were first reported by Kinard, Weichold, and Kirk[7] who demonstrated the feasibility of such a technique for the production of variable-area RTDs, but achieved only limited control over the area due to the material employed. Since then, Dellow *et al.*[8] and Guéret *et al.*[9] have produced this type of device on more suitable material and demonstrated significant variable-area operation. Both of these groups have reported fine structure in the characteristics close to threshold which they have attributed to single-electron tunneling through impurity states in the active region.[8,10–12] Guéret *et al.*[9,10] have also claimed evidence of lateral confinement effects in their smaller devices, although this finding has been questioned.[13]

While surface gates are clearly capable of producing variable-area RTDs, one possible disadvantage of this method of confinement is the asymmetry of the squeezing at the barriers resulting from the location of the surface gate, which tends to degrade the peak-to-valley (P/V) ratio of the devices.[14,15] The asymmetry can potentially be reduced by the use of in-plane gates, as reported for structures fabricated on two-dimensional electron gas (2DEG) material by Meirav *et al.*[16] and Blaikie *et al.*[17] This article presents results arising from the application of in-plane gate technology to RTD material to produce variable-area resonant tunneling diodes (VARTDs).

In the new structures, lateral confinement is produced by implanting and activating a p-type region in the n-type material surrounding the RTD device area. The resulting p-n junction between the implanted gate and the unimplanted device region is then reverse biased to give a depletion region, the size of which depends on the magnitude of the applied voltages. In this manner, an electrically controlled confinement potential is created around the active RTD area. Numerical modeling, described later, has predicted that the shape of this confinement potential should be more symmetric around the tunneling barriers than that produced in the surface-gated devices.

Using this design, in-plane gated variable-area RTDs have been produced for two materials and a range of device sizes. A full characterization has been performed on the material itself[18] and also on the gross characteristics of large-area devices. In relatively large area device characteristics, structure has been observed which can be attributed to single-electron tunneling through donor states in the active

 0021-8979/94/76(2)/1276/11/$6.00

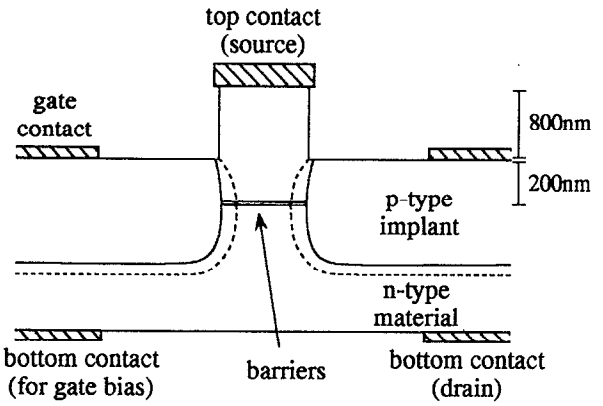

FIG. 1. Schematic cross-sectional diagram of the devices used in these experiments. The extent of the depletion region surrounding the p-type implant is indicated by the dashed line, and the bottom contacts have been displaced for clarity.

areas. Smaller devices have also been fabricated, to verify that reduced lateral dimensions can be produced by the process. Structure has been seen in the characteristics of the smallest devices that is consistent with (but not conclusively due to) the effects of lateral quantization in the RTD quantum well.

In this article, Sec. II describes briefly the design and fabrication of the devices used in the experiments. The operation of relatively large area devices is discussed in Sec. III, which is divided into six subsections, including: the operating range of the devices; their operation at 4.2 K; the modeling of the confinement potential produced by the implant; the shift of the resonance voltage seen in the smaller devices; and the fine structure seen around threshold. Section IV presents results obtained for small-area devices in which fine structure consistent with lateral quantization effects is seen. Results are also shown for devices with a strip, rather than a circular, geometry in which the observed characteristics can be attributed in part to a pinning of the confinement potential by donor sites close to the RTD barriers. Finally, Sec. V presents some conclusions.

II. DEVICE STRUCTURE

A schematic cross-sectional diagram of the devices used in these experiments is shown in Fig. 1. Current flows between the top and bottom contacts through the resonant-tunneling double barriers, with the area of the device being defined by a reverse-biased p-type region implanted into the bulk n-type material around the top contact. The width of the resulting depletion region, and hence the effective area of the device, depends upon the bias applied to the gate. An estimate of the depletion gives, for a background doping of 1×10^{16} cm^{-3} and a reverse bias of a few volts, a maximum depletion width of about 0.8 μm, showing that devices with fabricated dimensions around 1 μm are required for the variation in area to be significant.

A full description of the design and fabrication of these devices has been given elsewhere.[18,19] One of the most important factors to be considered is the design of the material.

TABLE I. Layer structures of the two materials used in the variable-area resonant tunneling diode experiments. All doping was n type, with Si.

Material	Doping (cm^{-3})	Material 1 layers (nm)	Material 2 layers (nm)
GaAs	5×10^{18}	130	150
GaAs	2×10^{17}	130	100
GaAs	8×10^{16}	170	150
GaAs	3×10^{16}	210	200
GaAs	1×10^{16}	380	350
GaAs	0.0	4.2	10.0
AlAs	0.0	4.2	5.0
GaAs	0.0	5.9	7.0
AlAs	0.0	4.2	5.0
GaAs	0.0	4.2	10.0
GaAs	1×10^{16}	380	350
GaAs	3×10^{16}	210	200
GaAs	8×10^{16}	170	150
GaAs	2×10^{17}	130	100
GaAs	5×10^{18}	420	500
		SI substrate	

In order to achieve a large variation in the depletion width at the device, a graded doping profile is adopted in which the concentration is reduced from 5×10^{18} cm^{-3} in the contact layers (adjacent to the surface and to the semi-insulating substrate) to 1×10^{16} cm^{-3} near the barriers. The grading occurs in several stages, over a distance of approximately 1000 nm. Such a profile is similar to that reported for the studies using surface-gated RTDs, and the reasoning behind this design has been discussed elsewhere.[8,19] Two materials with such graded doping were used in the experiments reported here; the layer structures of these, termed material 1 and material 2, are given in Table I. The most significant difference between the materials is in the thicknesses of the barrier and well layers: Material 1 has a significantly thinner double-barrier system and so exhibits a far higher resonance current with a consequently shorter average electron lifetime in the quantum well.

Both materials possess thick, low-doped layers adjacent to the double-barrier structures which alter the characteristics of the materials from those otherwise expected. In particular, a significant accumulation region is formed on the emitter (negatively biased) side of the barriers and a significant depletion region on the collector (positively biased) side. The voltage drop across this depletion region greatly increases the applied bias required for the RTD resonance condition. For material 1, resonance is found at 1.85 V rather than the 0.15 V expected for similar material without such a depletion region, while for material 2 resonance occurs at 0.67 V as opposed to 0.11 V. The accumulation region results in the formation of a triangular quantum well adjacent to the emitter barrier from which the majority of the tunneling into the quantum well between the barriers occurs. Thus, the principal tunneling in both materials is a 2D-to-2D process (for large-area devices) rather that the more usual 3D-to-2D process. Characteristics for both materials in forward bias (i.e., with the top contact layer positively biased with respect to the bottom contact layer) are shown in Fig. 2, which gives the results for large-area two-terminal devices at 4.2 K. Re-

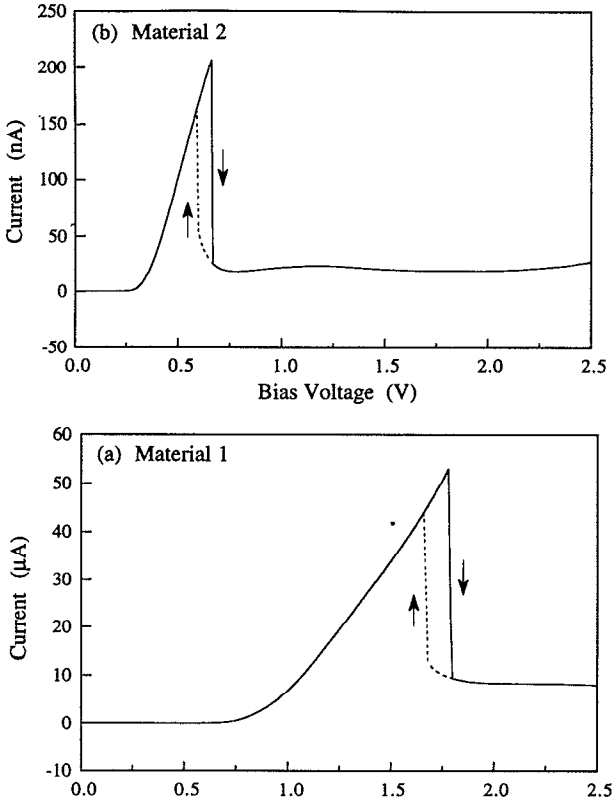

FIG. 2. Characteristics of the materials measured at 4.2 K using large-area two-terminal devices fabricated by wet etching. In both cases, the solid line shows the upward voltage sweep and the dashed line the downward sweep.

verse bias characteristics were found to be very similar, with only slight differences in the resonance voltages found due to the inevitable asymmetries in the growth of the double barriers. In both cases, significant hysteresis is seen (indicated by the dotted lines) which can be attributed to charge buildup in the quantum wells.[18]

The use of materials with such graded doping profiles causes difficulties in the fabrication due to the depth of the double barriers beneath the surface of the material (1000 nm) and the limited range of the implanted ions (300 nm). A pillar structure is produced by etching material from around the top contact, to ensure that the peak dose of the ion implant occurs at the level of the double barriers. The top ohmic contact metallization of the device is used as a self-aligned mask for subsequent process stages: for reactive ion etching of the pillar, and for the broad-beam implantation of the device area. An (optional) isotropic etch is also performed to produce a slight undercut to the device pillar (indicated in Fig. 1) which prevents leakage between the top contact and the p-type gate region that results from inadvertent but inevitable implantation down the side of the pillar structure. It was found that for the higher-current device in material 1 such an undercut was not required, whereas for material 2 leakage was more significant and the undercut was required for correct device operation.

III. LARGE-AREA DEVICE OPERATION

Large-area devices (with pad diameters ≥ 2 μm) have been fabricated on material 1, and these are useful for demonstrating the basic principles of operation of the VARTDs. None of the devices discussed in this section included the undercut etch discussed earlier, and so all show a relatively large gate leakage to the top contact. For all of the devices studied, the contact resistances and the material resistances were found to be negligible compared to the barrier and reverse-biased junction impedances.

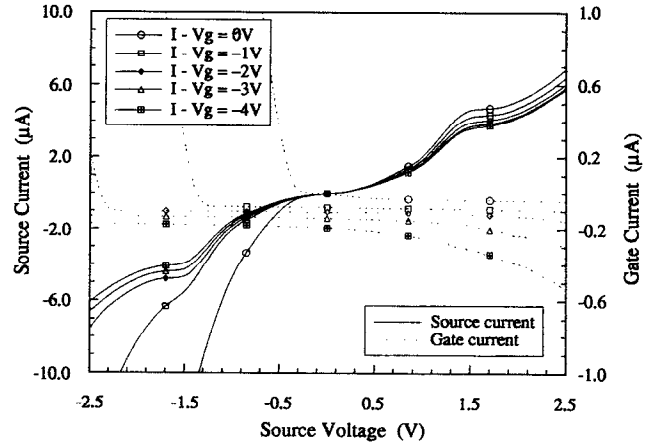

FIG. 3. Characteristics of a 4-μm-diam device at room temperature on material 1, showing the source current (solid lines) and the gate current (dashed lines) for various gate voltages.

Throughout this article the convention is used that the top contact is termed the "source" and the bottom contact the "drain," whatever the direction of current flow. The gate voltage is referenced to the drain of the device. Also, where device sizes are quoted, these refer to the lithographic diameters of the top contact pads and not to any measure of the actual electrical dimension (this being termed the "electrical device diameter").

A. Device operating range

The main restriction on the operating range of the devices is the range of gate and source voltages over which the leakage current through the p-n junction remains sufficiently small. In this context, three current components need to be considered: the current through the quantum well (the channel current); the current from the gate to the bottom n^+ region; and the current from the gate to the top n^+ region. Figure 3 shows the source and gate currents versus source voltage at various gate biases for a 4-μm-diam device at room temperature. Although the resonance effects are weak at this temperature (since thermal broadening is similar to the spacing of energy levels in the quantum well), the larger leakage currents which occur give a useful indication of the operating range.

As can be seen from the gate current, the bulk leakage can be high in these devices because of the large area of the bulk junction but, by using separate bottom n-type contacts for the gate and the channel connections, this current can effectively be decoupled from the source current measured through the top contact pad. The range of operating voltage is then given principally by the conditions for which the current between the gate and the top contact becomes signifi-

cant compared with the current through the resonant tunneling barriers. At one extreme this is due to the turn on of the p-n junction, while at the other it is due to reverse-bias breakdown. For the junction not to become forward conducting, and neglecting the (small) voltage drops due to any series resistances, the following condition must hold:

$$V_g - V_s \leq V_T, \tag{1}$$

where V_g is the gate voltage, V_s is the source voltage, and V_T is the junction threshold voltage. V_T can range from about 0.2 to 1.4 V, depending on the quality and abruptness of the junction. The device in Fig. 3 shows a value of V_T=0.4 V which is low due to the lack of an undercut to the top pad, resulting in a nonabrupt junction up the sides of the pillar. For devices in which an undercut pillar is incorporated, values of V_T around 1.2 V are found, much closer to the theoretical maximum and consistent with the more abrupt nature of the top p-n junction in such structures.

At the other extreme, device operation is impaired by the top leakage current resulting from the reverse-bias leakage or breakdown. Which of these mechanisms dominates depends again on details of the implant, but in general

$$V_s - V_g \leq V_{\mathrm{Br}} \tag{2}$$

where V_{Br} is the breakdown (or leakage) threshold. For all working devices in this study, V_{Br} was found to be between 4.0 and 6.0 V.

B. Device squeezing at 4.2 K

Devices with various diameters of the top pad have been fabricated on material 1, and typical characteristics for a 3-μm-diam VARTD at 4.2 K are shown in Fig. 4. Overall the features are as expected, with a reduction of peak current being seen for increasingly negative gate biases. Several features, however, require more detailed consideration.

It would be useful to calculate a value for the effective electrical device diameter versus gate voltage, and hence derive some idea of the amount of depletion occurring at the resonant tunneling barriers. At first sight, we might just use the peak current densities I_0 (measured using large, fixed-area devices) in the following equation:

$$I = I_0 \frac{\pi}{4} (D - x)^2 \tag{3}$$

where I is the peak current, D is the top pad diameter, and x is the effective depletion (dependent on gate voltage).

However, in contrast to the two-terminal device characteristics (Fig. 2), the VARTDs do not show any hysteresis and so it is not clear which value of the peak current density should be assumed (since this varies along the hysteresis curve). Instead, it is possible to use two similar devices of different dimensions to establish the peak current density. Assuming that the depletion width x is the same in both devices at a given gate voltage, Eq. (3) gives

$$I_0 = \frac{4}{\pi} \left(\frac{\sqrt{I_1} - \sqrt{I_2}}{D_1 - D_2} \right)^2, \tag{4}$$

where the subscripts refer to the two devices.

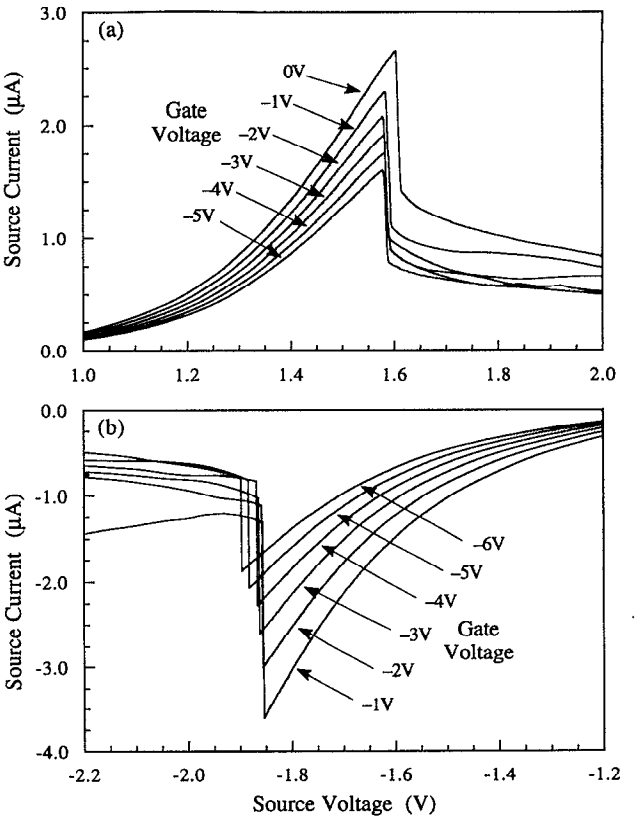

FIG. 4. Typical VARTD characteristics for a 3-μm-diam device at 4.2 K on material 1. In contrast to the fixed-area devices (Fig. 2), no hysteresis is seen in this case.

Applying this equation to results for devices fabricated on material 1 gives a value for the negative peak current density of 540±20 nA μm^{-2}, slightly below that of 588±20 nA μm^{-2} found elsewhere for two-terminal devices with charge buildup in the quantum well.[18] Similar measurements performed on material 2 give a value for the negative peak current density of 2.1±0.1 nA μm^{-2}.

This value for the peak current density can now be used in Eq. (3) to calculate the effective device diameters ($D-x$) as a function of gate voltage. The results of this for both 3- and 2-μm-diam devices are shown in Fig. 5. The most striking feature of this graph is the difference in the electrical diameters of the devices with the source positively and negatively biased with respect to the drain. The amount of squeezing depends on the voltage difference between the gate and the channel (the n-type region between the gate), and in the present material there is a large voltage drop along the channel at resonance which significantly affects this. For the measurement configuration used, the potential difference between the gate and the lower part of the channel remains constant in both forward and reverse source bias, whereas the potential difference between the gate and the upper part of the channel alters by approximately twice the resonance voltage. For the 3 μm device shown here this difference is about 3.4 V, with the greatest squeezing occurring when the source is forward biased. Assuming that the implant is symmetrical, we would therefore expect that the effective device diameters

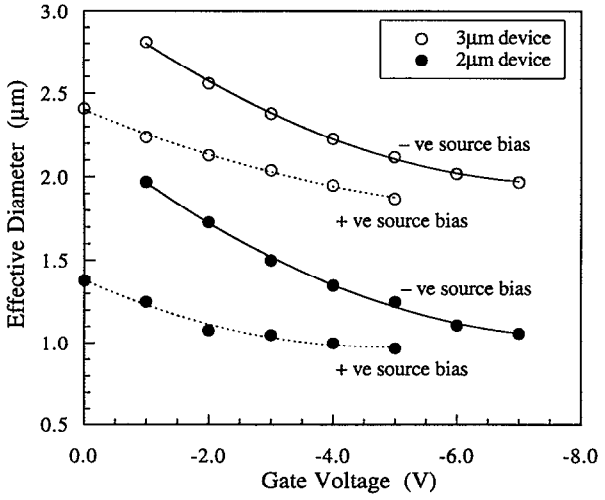

FIG. 5. Electrical diameters for 3 and 2 μm top pad diameter devices at 4.2 K on material 1. Results are shown for the source biased positively and negatively with respect to the drain.

for the 3 μm diode under forward and reverse bias would show a similar form, but be displaced by a gate voltage of about 3.4 V. The results in Fig. 5 are consistent with this.

Additional experimental evidence for the symmetry of the gate around the barriers is given by the peak-to-valley (P/V) ratios of the VARTDs. Previous work on surface-gated variable-area diodes has found that the P/V ratio in one bias remained roughly constant while in the other bias the ratio diminished rapidly with applied gate voltage.[14] The authors attributed this to a gate-voltage-dependent asymmetry in the lateral confinement potential, resulting from the asymmetrically placed gates. For the implanted gates used here, however, the P/V ratio shows similar characteristics in both the forward- and reverse-biased directions. For example, for a 2 μm device at 4.2 K, the P/V ratio varies from 2.6 to 2.3 in reverse bias and from 2.5 to 2.2 in forward bias. Overall, the ratio is degraded from the large-area value of 5.9 due to the depletion asymmetry on the collector side of the barriers, and this degradation becomes slightly greater for increasingly negative gate voltages. However, the amount of degradation is similar for both the positive and negative source biases, indicating that the underlying implant itself is symmetrical close to the barriers.

C. Modeling of gross characteristics

To investigate the effects of the implant further, the system has been modeled using the HIHEART classical simulation package at the Central Research Laboratories, Hitachi Ltd.[20,21] This enables the full geometry of the pillar structures, the graded doping profiles of the material, the variation in implant concentration with depth, and the effects of lateral ion spreading to be included, although it does not take proper account of the quantum-mechanical effects around the barriers. The potential distribution in a 2-μm-diam device is shown in Fig. 6 for two gate biases, with the results obtained agreeing well with those expected. Overall, the lateral squeezing produced by the implantation is symmetrical

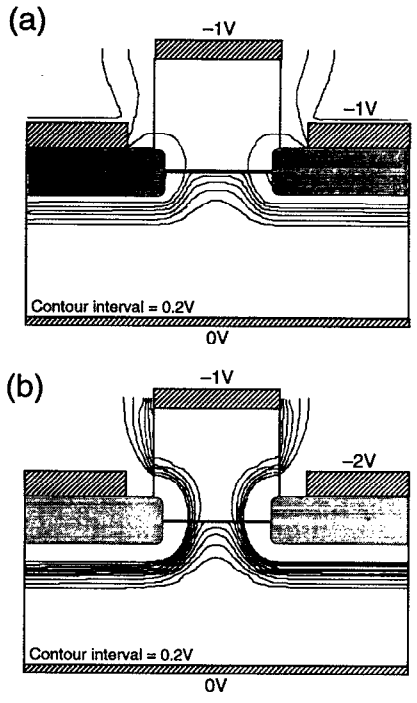

FIG. 6. Potential distributions in a 2-μm-diam device produced using the HIHEART modeling package (a) with a gate bias of -1 V, and (b) with a gate bias of -2 V. The shaded areas indicating the implanted regions are schematic only.

around the barriers. However, there is a slight asymmetry which arises as a result of the collector depletion region, and this might be expected to degrade the P/V ratios. This asymmetry becomes greater as the gate bias is increased further, consistent with the increasing degradation of the P/V ratio. The large potential drop across the collector depletion region can also clearly be seen.

Modeling such as this can also be used to optimize the design of the material for future studies. In particular, for the materials currently under investigation, the great majority of the squeezing actually occurs in the two lowest doped layers adjacent to the barriers, and this would allow a reduction in thickness or removal of some of the higher doped layers in the graded material.

D. Voltage shift of resonance position

The characteristics for the 3 μm device (Fig. 4) show slight shifts in the resonance voltage, especially noticeable for the higher gate biases in (b). These voltage shifts become greater as the device size is reduced. The most straightforward explanation for such a shift would be an area-dependent series resistance. However, this would also be expected to produce hysteresis in the I-V characteristics, which was not observed. Also, the effective series resistance is not linearly related to the reciprocal of the area, indicating that the simple picture of a series resistance is not correct.

Figure 7 shows the potential along the centre of the channel of a 2 μm device given by the numerical model for various gate biases. Even at the center of the channel, the energy of the conduction band in the depletion region (and

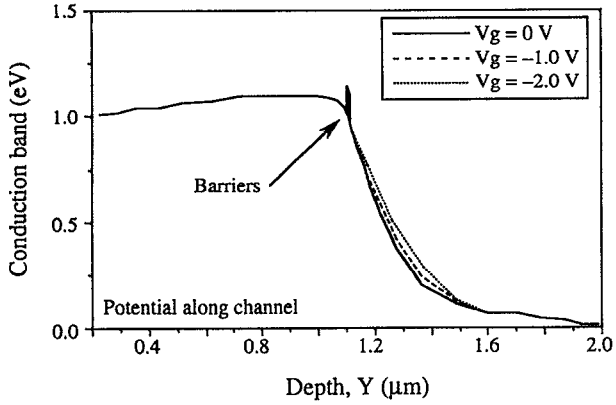

FIG. 7. Conduction-band energy along the center of a 2-μm-diam device given by the HIHEART modeling package. The potential in the collector depletion region is affected by the gate bias even at the center of the channel.

also in the well) is raised as the gate bias becomes increasingly negative, in a similar manner to that reported by Reed *et al.* for their small-area etched devices.[3] Although detailed numerical comparisons between the modeled shifts and experimental results have yet to be made, we believe that the mechanism described above is responsible for the observed shifts in the resonance voltage.

E. Device operation at 77 K

The high-current-density material 1 is capable of showing resonance effects at temperatures up to 300 K, so the main limiting factor on device operation is the p-n junction leakage current. Operation at 77 K was found to be fully satisfactory, as shown in Fig. 8. Thermal broadening has led to a rounding of the negative differential resistance region, and the shift of the resonance voltage with applied gate voltage is less than for the same device at 4.2 K. This is consistent with the reason previously suggested for the shift, since at the higher temperatures less of the collector side of the device will be depleted, and so the applied gate bias will

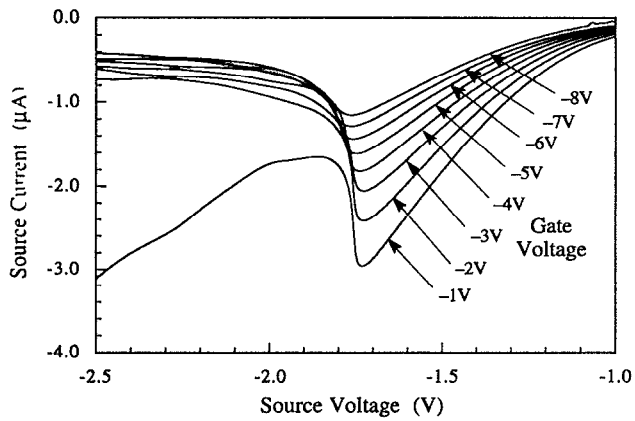

FIG. 8. Characteristics of a 3-μm-diam device at 77 K on material 1, showing a similar gate action to that at 4.2 K. The effects of the p-n junction turn on and reverse breakdown can be seen on the curves for $V_g = -1$ and -8 V, respectively.

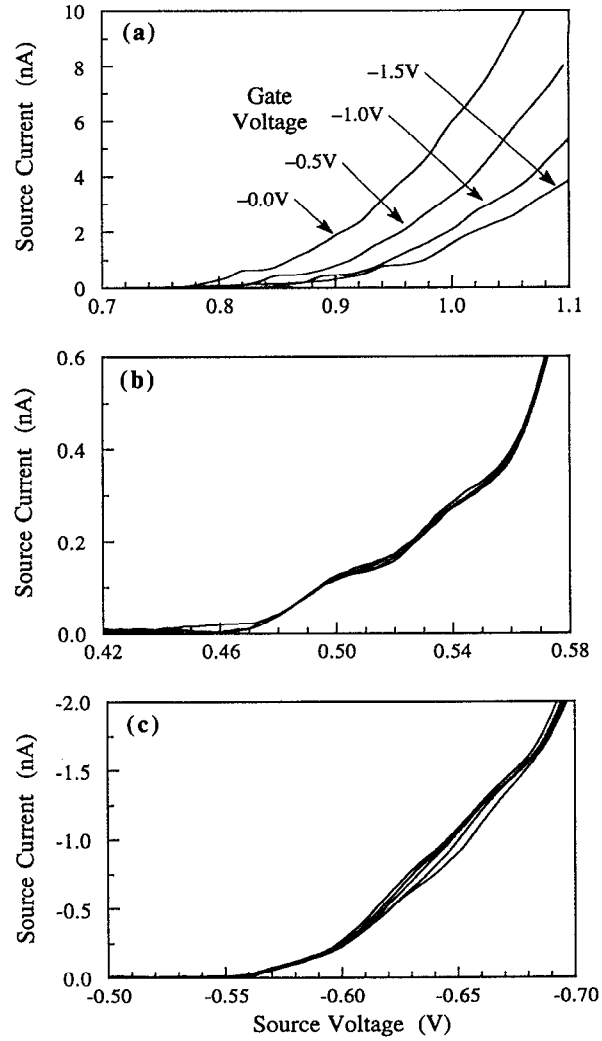

FIG. 9. Fine structure at threshold voltage for VARTD devices on material 1 at 4.2 K, (a) for a forward-biased 2 μm device, (b) for a forward-biased 4 μm device, and (c) for a reverse-biased 4 μm device.

have a smaller effect. Overall, the peak current is slightly reduced at the higher temperatures, possibly due to broadening of the depletion region associated with the reverse-biased p-n junction; however, the device operation is otherwise very similar to that at 4.2 K and a similar degree of control over the device area is achieved.

F. Tunneling through donor states

The minimum pad diameter for the working devices fabricated on material 1 was 2 μm, giving a range of active device diameters from about 1 μm upward, all of which are too large to show the effects of lateral confinement. Nevertheless, fine structure was seen for all these devices around the threshold voltage, even at a relatively high temperature of 4.2 K. Typical characteristics are shown in Fig. 9 for a 2-μm-diam device in forward bias and for a 4-μm-diam device in forward and reverse bias. These show a weak series of plateaux close to the device threshold. For the 2 μm de-

vice the position of these is dependent on gate voltage, while for the larger devices this is not the case. Also the structure is different in forward and reverse biases.

One of the clearest features is the dependence of the plateau position on gate voltage for the 2 μm device. For smaller structures this might be taken as evidence for lateral confinement,[9] but the devices here are too large for this to be the case. In fact, a similar positional dependence on gate voltage has already has been seen with the resonance voltage of the 2 μm device, which was attributed to the effect of the gate bias on the collector depletion region. This mechanism can also apply here, and the voltage shift of the fine structure can be thought of as an artefact of the depletion region in the material rather than a property of the fine structure itself. Such results call into question the use of a shift in fine structure with applied gate bias as the sole proof of lateral confinement effects.

Several possibilities exist for the origin of the fine structure. The first, lateral confinement, can be discounted due to the size of the devices and the invariance of the effect on gate bias (for the larger devices). An alternative mechanism might be Coulomb blockade. This, too, should show a strong dependence on device area and hence on gate bias. Furthermore, for Coulomb blockade to be observed, the electrostatic charging energy must be greater than the thermal broadening. For the temperature here (4.2 K) this gives the requirement that the device capacitance should be less than 10^{-16} F. An estimate of the capacitance of the present barrier system gives a minimum capacitance of 10^{-14} E, clearly ruling out the possibility of Coulomb blockade being observed in these devices at 4.2 K.

The final possibility for the origin of the structure is tunneling through donor or impurity states in the active region of the device, as has been discussed in several papers by Dellow *et al.*[8,11,12] for a variable-area RTD confined by the depletion region from a surface gate. An ionized donor in the quantum well gives rise to a localized potential well and associated bound states through which electron tunneling can occur for biases below the threshold voltage. The binding energy of such states depends on the position of the donors, with a maximum occurring for donors in the center of the well. Using modeled results by Greene and Bajaj,[22] this maximum binding energy can be estimated to be about 14 meV for the present system. For large-area devices containing numerous such donors, the spread in energies due to their random distribution in the well leads to any structure becoming washed out. However, for small devices with only a single or few donors, fine structure is expected around threshold as electrons tunnel through the bound states associated with the ionized donors.

The strongest structure is expected if only one donor is involved in the tunneling process. The plateau current I can be expressed as

$$I=\frac{ne}{\tau_w}, \tag{5}$$

where n is the number of electrons involved, e is the electronic charge, and τ_w is the electron lifetime in the quantum well. For single-electron tunneling n is unity.

TABLE II. Details of the fine structure seen close to threshold for three VARTD devices and the calculated carrier lifetimes in the quantum well assuming single-electron tunneling. The active device volume (between the RTD barriers) is also given.

Top pad diameter (μm)	First plateau current (pA)	First plateau voltage (mV)	Calculated lifetime (ps)	Active device volume (m^3)
2	500	820	320	0.6×10^{-20}
3	250	560	640	2.1×10^{-20}
4	150	500	1500	4.6×10^{-20}

Table II shows for three VARTD devices the currents and voltage positions of the first plateaux of the fine structure, the calculated lifetimes, and some physical dimensions. The calculated lifetimes correspond reasonably well to the approximate value of 500 ps derived for the large-area devices at resonance, indicating that the plateaux can be attributed to single-electron or few-electron tunneling. One possible mechanism for the apparent dependence of lifetime on device size is the changing electric field across the collector barrier resulting from the action of the gate on the collector depletion region: for smaller devices the field is greater (indicated by the higher voltage for the first plateau) and the carrier lifetime in the well correspondingly shorter. The total number of donor states expected in the quantum well can be estimated from the background doping density and the active device volume. Assuming a background doping of 10^{14} cm^{-3} this gives an estimate of one to five donor sites in the three device sizes considered here, which again is consistent with the picture of single-electron or few-electron tunneling.

The position of a single donor state in the well is random. Since the symmetry of the forward- and reverse-bias characteristics depends upon the donor being positioned in the center of the quantum well, there is a high probability of the characteristics showing asymmetry, as is observed. For cases involving more than one donor site, the first plateau will be due to the state with the lowest energy, produced by the donor site closest to the center of the well. This results in the gate bias having only a weak effect on the first plateau. The later structure will be due to a combination of higher states of the most central donor along with the first states of other outlying donor sites, and so we would expect the gate bias to have a greater effect. Indications of this type of behavior can be seen in Fig. 9, notably in graph (c). Unfortunately, due to the unknown and varying amount of voltage drop across the collector depletion region, it is not easy to compare energy levels and measured voltages, as performed by Dellow *et al.*[8]

In principle these effects should not be limited to the VARTD structures. For this reason, the characteristics of fixed-area two-terminal devices, fabricated for characterization of the material, have been measured in detail around threshold. As predicted, some very weak fine structure was observed in these devices, consistent with the larger active areas. Fine structure could still just be extracted from the data for devices with active areas up to 1.5×10^{-10} m^2, corresponding to about 100 donor sites in the active region between the barriers.

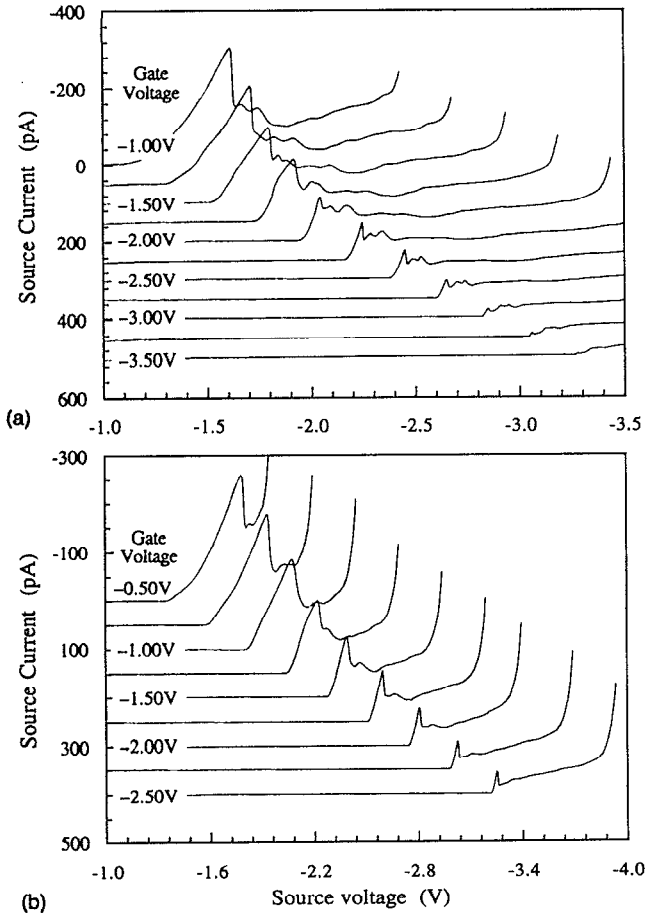

FIG. 10. Characteristics of (a) 1.4- and (b) 1.2-μm-diam devices on material 2 at 4.2 K. Successive curves have been displaced downward from zero for clarity.

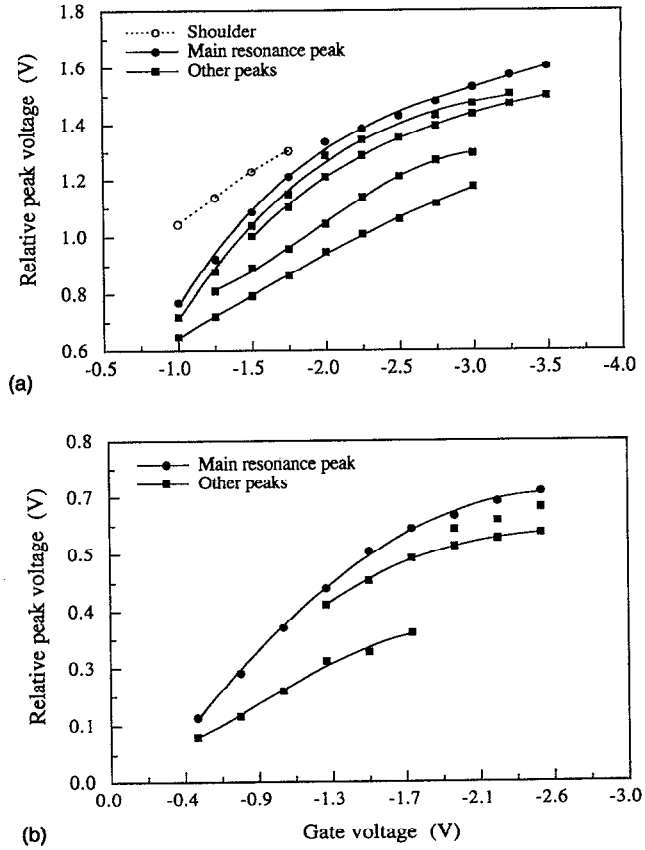

FIG. 11. Peak positions relative to the p-n junction threshold voltage vs gate voltage for (a) 1.4- and (b) 1.2-μm-diam devices on material 2 at 4.2 K. The corresponding I-V characteristics are shown in Fig. 10.

IV. SMALL-AREA DEVICE OPERATION

Following the basic characterization of the large-area devices, a range of VARTDs with top pad diameters less than 2.0 μm has been fabricated to study possible lateral confinement effects, with material 2 being used to give a longer carrier lifetime in the quantum well. Due to the low currents it was necessary to reduce the leakage to the top contact by using the undercut etch described earlier.

A. Characteristics of circular devices

Results for the large-area devices show that the depletion region associated with the reverse-biased p-n junction can be controlled between about 100 and 400 nm from the projected edge of the top pad. As the device diameters are reduced, the radius of curvature of the junction becomes smaller and so we would expect the depletion effect to become greater. Thus, it should be possible to pinch off completely devices with top pad diameters about 1 μm.

The characteristics for 1.4- and 1.2-μm-diam devices are shown in Fig. 10, with successive curves being displaced downward from zero for clarity. Only the reverse-bias characteristics are shown, since due to the asymmetry of the measurement configuration no conduction occurred with the source positively biased. Devices with pad diameters of 1.0 μm failed to conduct in either direction. Similar and contrasting features are seen in the two devices. As the gate reverse bias is increased, both devices show a reduction in the resonant current and an increase in the resonance voltage, along with a sharpening of the main resonance peak and extra structure in the valley current. However, the 1.2 μm device shows a reasonably constant P/V ratio, in contrast to the rapidly degrading ratio of the 1.4 μm device—a difference attributed to the implantation for the 1.4 μm device being asymmetric about the barriers due to a slight error in fabrication.

The voltage position of the observed fine structure can be determined relative to the p-n forward-bias thresholds (seen in the graphs). Due to the unknown size of the depletion region on the collector side of the barriers, the absolute voltages of the peaks are not meaningful; however, the p-n threshold relates the source (emitter) voltage to the gate voltage, and so can be used as a reference point. Using this property, the energy of any levels responsible for the fine structure can be related to the energy of the emitter levels by considering the relative voltages between the p-n junction turn-on threshold and any observed structure. Values of relative peak voltage versus gate voltage are plotted for the observed peaks of both devices in Fig. 11, in which the connecting lines are arbitrary. Both devices show some splitting of the structure up to a gate voltage of about -2.0 V, fol-

lowed by a common shift in the relative peak positions. Although the interpretation of this extra structure is not yet conclusive, some comments can be made.

The devices show a sharpening of the principal resonance with increasingly negative gate biases, and for the 1.4 μm device a shoulder is seen on the low-voltage side of the principal resonance [indicated by the open circles in Fig. 11(a)] which can be attributed to 3D delocalized emitter states above the 2D emitter states in the contact layers. The main interest in the fine structure is whether it could be due to lateral confinement effects.[6,23] To investigate this possibility, the lateral confinement potential has been modeled, and the results of this show that the lateral-confinement potential is roughly parabolic at the barriers. As the gate bias is increased, the lateral confinement becomes progressively narrower until at about -2.0 V (for the 1.4 μm device) a minimum size is reached after which the lateral-confinement well is simply shifted upward in energy without altering shape. Such a result appears consistent with the observations of a splitting of levels followed by a uniform shift. The modeling also predicts the increased splitting and earlier leveling of the results obtained for the smaller (1.2 μm) device, as seen.

An approximate calculation can be performed to estimate the magnitude of the expected splitting of levels. The energy levels in a harmonic potential are given by

$$E_n=(n+\tfrac{1}{2})\hbar\sqrt{K/m^*}, \tag{6}$$

where the well is of the form

$$V=\tfrac{1}{2}Kx^2, \tag{7}$$

and x is the distance coordinate, and K is a constant defined by Eq. (6).

Using the results of the HIHEART model for the 1.4 μm device, this gives a level splitting of about 5.5 meV at $V_g=-1.5$ V. The measured voltages can be calibrated to the energies in the well by the energy level associated with the large-area RTD resonance, and this then predicts a measured splitting of about 150 mV, consistent with that observed in Fig. 11.

The consistency of the observations with lateral confinement does not exclude the possibility that they could be due to some other mechanism. In particular, results very similar to those in Fig. 10(a) for the 1.4 μm device have been reported by Dellow *et al.*[15] for which the lateral confinement mechanism was discounted. Further experiments are needed on this point. Whatever the outcome of these, however, these results have clearly demonstrated the use of implanted-gate VARTDs to produce systems in which the lateral confinement effects become significant.

B. Discussion of fine structure

As indicated in Fig. 6, the lateral confinement produced by the implanted-gate technique is relatively uniform around the barrier and quantum-well layers. Indeed, this is a feature unusual to these devices. In surface-gated RTDs the depletion originates at an asymmetrically placed Schottky barrier, and this can result in a significant variation of the confinement across the RTD structure.[15] Even in uniformly etched pillar devices the different amounts of surface depletion in the well and contact layers give rise to a necked confinement potential.[24] The question of uniform or nonuniform confinement has important consequences for the form of the fine structure that might be seen and so is briefly considered here.

Much theoretical work has now been performed on the question of resonant tunneling through laterally confined devices, with a common statement being made that fine structure is observed only for cases in which there is nonadiabatic transport through the system, so that quantum mechanically the lateral modes in the system are not conserved.[25,26] In the context of the devices under consideration here, nonadiabatic transport will occur if the change in lateral confinement occurs on a length scale of the same order or less than the wavelength of the electrons in the system, which at resonance is approximately equal to the width of the quantum well. Thus, the question arises whether any additional fine structure might be expected in the implanted-gate laterally confined devices in which transport is largely adiabatic. This has been addressed in the context of this project by a three-dimensional numerical simulation of the quantum transport processes in zero-dimensional resonant tunneling diodes.[24,27] This has been applied to idealized 0D cases with both uniform and nonuniform ("hourglass") confinement potentials, leading to adiabatic and nonadiabatic transport, respectively. While the actual materials and dimensions used in the simulations are different from the proposed VARTD device structures, the principles are the same in both systems.

The forms of the I-V characteristics predicted for the two cases are quite different. For the hourglass confinement potential (nonadiabatic transport), both lateral-mode-conserving and nonlateral-mode-conserving channels are available, and both types contribute to the fine structure at zero temperature. The energy spacing of the mode-conserving levels is significantly less than that for the non-mode-conserving channels, so that as the temperature is raised the effects of the mode-conserving channels are lost first. Thus, the effect of the nonuniform confinement on the I-V characteristics is twofold: It leads to a more complex fine structure at very low temperatures, and some of the fine structure (that due to the non-mode-conserving tunneling processes) survives to higher temperatures than is the case for uniform confinement. This temperature dependence may be the origin of the statement that fine structure is only seen in laterally nonuniform situations.

The simulation, in agreement with other models,[26] therefore shows that, while fine structure due to the lateral quantization effects is expected to be small in uniformly confined devices, some structure will still exist. Of course, the question remains as to whether this can be observed, but if it can then this should allow the direct observation of adiabatic effects uncomplicated by the extra non-mode-conserving features.

C. Characteristics of strip devices

The final device geometry to be considered is the strip VARTD, in which the top pad, rather than being circular in plan, takes the form of a long narrow rectangle. The motiva-

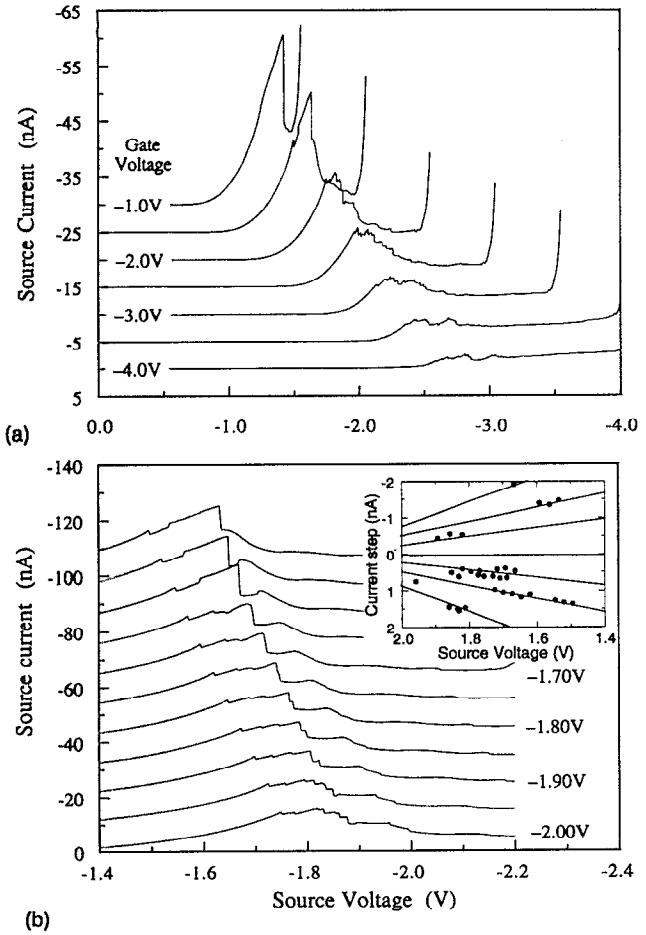

FIG. 12. Characteristics of a 1×100 μm^2 strip VARTD on material 2 at 4.2 K. Graph (b) shows a more detailed section for gate voltages between -1.5 and -2.0 V in 0.2 V steps, and the inset plots the heights of the observed current steps vs the source voltage. In both (a) and (b) successive curves have been offset from zero for clarity.

tion for using such a geometry is to increase the total device current while still maintaining a large amount of control over the device area.

The characteristics of a 1×100 μm^2 device on material 2 at 4.2 K are shown in Fig. 12. As expected for a device in which one dimension is small, a large amount of control is achieved over the current; however, in contrast to the smooth reduction of peak current in the small circular devices, the resonance peak breaks up into numerous smaller peaks at differing source voltages. Such characteristics are fully repeatable with time and thermal cycling, and were seen for all narrow devices of this type. Figure 12(b) shows a more detailed view for a smaller range of gate biases. On this scale the structure appears less random, with trends being seen for the positions of the current peaks. The heights of the current steps have been measured and are plotted versus the source voltage in the inset, and this shows that they fall roughly into multiples of some unit current step that is source voltage dependent.

A value for the unit step can be derived from the inset. Taking as an example the bias $V_s=-1.8$ V, the graph gives a unit current step of order 500 pA. This current I can then be related to the number of electrons associated with the step n by Eq. (5). Using the mean value for electron lifetime measured for large-area devices, this gives the number of electrons associated with the unit current step as about 300, which clearly eliminates the possibility of the steps being due to single-electron tunneling effects. At first, it was thought that this additional structure might be due to lateral confinement in the quantum well, although the number of features present might make this seem unlikely; however, a graph of the position of the structures versus gate voltage failed to show any positional splitting of the steps with increasing confinement.

To account for the observed characteristics, it is required that the resonance peak position increasingly depends on gate voltage as the degree of confinement is increased. Such a mechanism has previously been discussed with reference to the smaller circular devices in Sec. III D, in which the positional dependence of the resonance peak was attributed to the effect of the gate potential on the collector depletion region; however, this would be expected to give a uniform shift, and therefore cannot alone account for the numerous observed peaks which indicate a varying confinement potential along the device. This could be due simply to variations in the width of the original top pad, but then the effects would be expected to be largely random and therefore not to result in quantized current steps. Also, the effects of any such variation would be expected to become smoothed by the action of the implantation and depletion region at the depth of the barriers. Thus a mechanism is proposed in which the nonuniformities that give rise to the varying confinement potential along the strip devices are due to donor sites in the depletion region close to the barriers.

The lateral confinement is a nontrivial function of the source, gate, and drain potentials, but close to the barriers is mainly dependent on the difference between the source and gate voltages. As this difference increases, the lateral confining potential becomes narrower but, if there is a donor site in the depletion region, one wall of the confining potential may become pinned. Eventually the applied potential will become great enough to overcome the pinning and a sudden step in confining potential will occur, producing a corresponding step change in the resonance conditions at that point. The magnitude of the resulting current step depends upon the area of the device involved, and so can correspond to many electron tunneling events, as observed. The source-gate voltage at which the pinning is overcome varies with the position of the donor concerned, and in the long strip a number of donors can result in numerous steps at various voltages, also as seen. If two or more pinning centers are close enough to be coupled, then multiples of the unit current step or bistable regions may occur.

An estimate of the number of donor sites in the depletion region close to the barriers yields, for a background doping of 10^{14} cm^{-3} and effective range of 100 nm (since no effect is seen in the devices of width 300 nm), approximately 100 donors for a device of this size. This is the correct order for the number of unit current steps observed in the characteristics at the higher gate voltages. As required, the voltage

spread of the step structures is seen to increase as the degree of lateral confinement at the depletion region becomes greater.

V. CONCLUSIONS

This article has presented results from the novel application of implanted in-plane gate technology to resonant tunneling material to produce variable-area resonant tunneling diodes. Measurements performed on relatively large-area devices have indicated that the lateral confinement produced by such a technique is inherently symmetric about the RTD barriers, a finding supported by numerical modeling of the devices. Fine structure has been observed at 4.2 K close to the threshold voltage even in the large-area devices, and this has been attributed to single-electron or few-electron tunneling through donor states in the quantum well. Small-area devices, in which the effects of lateral quantization might be expected, have also been studied and additional fine structure has been observed in the valley currents. The splitting of this structure with increasing confinement has been shown to be consistent with the effects of lateral confinement. Finally, results have been presented for strip devices which show fragmentation of the resonance peak that has been attributed to the effects of pinning of the confinement potential by donors close to the active regions of the devices.

ACKNOWLEDGMENTS

The authors wish to thank R. J. Blaikie and S. Blythe for help with some aspects of the fabrication of the devices, and T. Tanoue for providing some of the material used in the experiments. C.J.G. acknowledges support by the Science and Engineering Research Council.

[1] M. A. Reed, J. N. Randall, and J. H. Luscombe, Nanotechnology **1**, 63 (1990).
[2] B. Su, V. J. Goldman, and J. E. Cunningham, Phys. Rev. B **46**, 7644 (1992).
[3] M. A. Reed, J. N. Randall, R. J. Aggarwal, R. J. Matyi, T. M. Moore, and A. E. Wetsel, Phys. Rev. Lett. **60**, 535 (1988).
[4] S. Tarucha and Y. Hirayama, Phys. Rev. B **43**, 9373 (1991).
[5] M. Tewordt, L. Martín-Moreno, T. J. Nicholls, M. Pepper, M. J. Kelly, V. J. Law, D. A. Ritchie, J. E. F. Frost, and G. A. C. Jones, Phys. Rev. B **45**, 14 407 (1992).
[6] S. Tarucha, Y. Hirayama, T. Saku, and T. Kimura, Phys. Rev. B **41**, 5459 (1990).
[7] W. B. Kinard, M. W. Weichold, and W. P. Kirk, J. Vac. Sci. Technol. B **8**, 393 (1990).
[8] M. W. Dellow, P. H. Beton, C. J. G. M. Langeral, T. J. Foster, P. C. Main, L. Eaves, M. Henini, S. P. Beaumont, and C. D. W. Wilkinson, Phys. Rev. Lett. **68**, 1754 (1992).
[9] P. Guéret, N. Blanc, R. Germann, and H. Rothuizen, Phys. Rev. Lett. **68**, 1896 (1992).
[10] P. Guéret, N. Blanc, R. Germann, and H. Rothuizen, Semicond. Sci. Technol. B **7**, B462 (1992).
[11] M. W. Dellow, C. J. G. M. Langerak, P. H. Beton, T. J. Foster, P. C. Main, L. Eaves, M. Henini, S. P. Beaumont, and C. D. W. Wilkinson, Superlattices and Microstructures **11**, 149 (1992).
[12] M. W. Dellow, C. J. G. M. Langerak, P. H. Beton, T. J. Foster, P. C. Main, L. Eaves, M. Henini, S. P. Beaumont, and C. D. W. Wilkinson, Surf. Sci. **263**, 438 (1992).
[13] P. H. Beton, L. Eaves, and P. C. Main, Phys. Rev. Lett. **69**, 2995 (1992) (comment); P. Guéret, N. Blanc, R. Germann, and H. Rothuizen *ibid.* (reply).
[14] P. H. Beton, M. W. Dellow, P. C. Main, T. J. Foster, L. Eaves, A. F. Jezierski, and M. Henini, Appl. Phys. Lett. **60**, 2508 (1992).
[15] M. W. Dellow, P. H. Beton, P. C. Main, T. J. Foster, L. Eaves, A. F. Jezierski, W. Kool, M. Henini, S. P. Beaumont, and C. D. W. Wilkinson, Semicond. Sci. Technol. **7**, B442 (1992).
[16] U. Meirav, M. A. Kastner, M. Heiblum, and S. J. Wind, Phys. Rev. B **40**, 5871 (1989).
[17] R. J. Blaikie, J. R. A. Cleaver, H. Ahmed, and K. Nakazato, Appl. Phys. Lett. **60**, 1618 (1992).
[18] C. J. Goodings, Ph.D. thesis, Cambridge University, 1993.
[19] C. J. Goodings, J. R. A. Cleaver, and H. Ahmed, Electron. Lett. **28**, 1535 (1992).
[20] T. Ohtoshi, K. Yamaguchi, C. Nakaoka, T. Uda, Y. Murayama, and N. Chinone, Solid-State Electron. **30**, 627 (1987).
[21] H. Mizuta, K. Yamaguchi, M. Tanoue, and S. Takahashi, IEEE Trans. Electron Devices **ED-36**, 2307 (1989).
[22] R. L. Greene and K. K. Bajaj, Solid State Commun. **45**, 825 (1983).
[23] B. Su, V. J. Goldman, M. Santos, and M. Shayegan, Appl. Phys. Lett. **58**, 747 (1991).
[24] H. Mizuta, C. J. Goodings, M. Wagner, and S. Ho, J. Phys. Condens. Matter **4**, 8783 (1992).
[25] G. W. Bryant, Phys. Rev. B **39**, 3145 (1989).
[26] G. W. Bryant, Phys. Rev. B **44**, 12837 (1991).
[27] H. Mizuta and C. J. Goodings, J. Phys. C **3**, 3739 (1991).